Drosophila Dosage Compensation Involves Enhanced Pol II Recruitment to Male X-Linked Promoters

12. M. J. Santander-Ortega, A. B. Jódar-Reyes, N. Csaba, D. Bastos-González, J. L. Ortega-Vinuesa, *J. Colloid Interface Sci.* **302**, 522 (2006).
13. M. Santander-Ortega, N. Csaba, M. Alonso, J. Ortega-Vinuesa, D. Bastos-González, *Colloids Surf. A Physicochem. Eng. Asp.* **296**, 132 (2007).
14. A. K. Chauhan et al., *J. Exp. Med.* **203**, 767 (2006).
15. W. Bergmeier et al., *Proc. Natl. Acad. Sci. U.S.A.* **103**, 16900 (2006).
16. H. Ni et al., *J. Clin. Invest.* **106**, 385 (2000).
17. P. S. Frenette et al., *Blood* **91**, 1318 (1998).
18. R. Gref et al., *Science* **263**, 1600 (1994).
19. J. C. Murciano et al., *Am. J. Physiol. Lung Cell. Mol. Physiol.* **282**, L529 (2002).
20. J. A. Straub, D. E. Chickering, T. G. Hartman, C. A. Gloff, H. Bernstein, *Int. J. Pharm.* **328**, 35 (2007).
21. M. Di Marco et al., *Int. J. Nanomedicine* **5**, 37 (2010).
22. S. Rana, Y. C. Yeh, V. M. Rotello, *Curr. Opin. Chem. Biol.* **14**, 828 (2010).
23. J. C. Murciano et al., *Nat. Biotechnol.* **21**, 891 (2003).
24. K. Danielyan et al., *Circulation* **118**, 1442 (2008).
25. K. Ganguly et al., *J. Pharmacol. Exp. Ther.* **316**, 1130 (2006).

Drosophila Dosage Compensation Involves Enhanced Pol II Recruitment to Male X-Linked Promoters

Thomas Conrad,[1]* Florence M. G. Cavalli,[2]* Juan M. Vaquerizas,[2] Nicholas M. Luscombe,[2,3,4,5]† Asifa Akhtar[1]†

Through hyperacetylation of histone H4 lysine 16 (H4K16), the male-specific lethal (MSL) complex in *Drosophila* approximately doubles transcription from the single male X chromosome in order to match X-linked expression in females and expression from diploid autosomes. By obtaining accurate measurements of RNA polymerase II (Pol II) occupancies and short promoter-proximal RNA production, we detected a consistent, genome-scale increase in Pol II activity at the promoters of male X-linked genes. Moreover, we found that enhanced Pol II recruitment to male X-linked promoters is largely dependent on the MSL complex. These observations provide insights into how global modulation of chromatin structure by histone acetylation contributes to the precise control of Pol II function.

In *Drosophila* males, the histone acetyltransferase MOF (males absent on the first) within the MSL (male-specific lethal) complex mediates global hyperacetylation of X-linked chromatin at histone H4 Lys[16] (H4K16) (*1*, *2*). The mark is thought to mediate a doubling of X-linked transcription by promoting the formation of an accessible chromatin structure (*3–6*). However, the mechanism of this activation has remained elusive. It has been proposed that dosage compensation occurs by enhanced transcription elongation through male X-linked genes (*7*, *8*), although direct support for this claim is limited.

The study of dosage compensation has been complicated by the relatively small (factor of 2) increase in transcription rate and by the widespread use of aneuploid male cell lines as the model system. A shortcoming has been the lack of direct comparison of RNA polymerase II (Pol II) occupancies between male and female flies. Without reference measurements in females, sex-specific and gene-specific effects cannot be distinguished and unambiguous conclusions about the dosage compensation mechanism are impossible.

Chromatin immunoprecipitation sequencing (ChIP-seq) experiments for the Rpb3 subunit of Pol II were performed in male and female third-instar larva salivary glands (table S1 and figs. S1 and S2). We integrated these measurements with ChIP-seq data for MOF, histone H4, and acetylated H4K16 (H4K16ac) from the same tissues (*9*). We clustered 1360 autosomal and 242 X-linked genes with significant Pol II occupancies along the full transcribed regions according to their H4K16ac status in males (Fig. 1A and fig. S3). As expected, binding by the acetyltransferase MOF correlated with the occurrence of H4K16ac. Moreover, although the histone mark extends across the entire lengths of genes on the male X chromosome, it is restricted to gene promoters on the male autosomes and on all female chromosomes (*10*).

A comparison of Pol II occupancies between the gene clusters in male and female samples reveals the difference in transcriptional output achieved through dosage compensation (Fig. 1B

and fig. S4). There is a clear enrichment of Pol II levels among hyperacetylated genes on the male X chromosome; this enrichment is maintained throughout the entire length of genes, including promoter regions [defined as transcription start site (TSS) –300 base pairs (bp) to TSS +500 bp], transcribed regions [TSS +500 bp to polyadenylation site (PolyA) –500 bp], and 3′ ends (PolyA –500 bp to PolyA +300 bp). These results support the strong correlation between chromosome-wide H4K16ac and increased transcriptional activity on the male X chromosome.

To identify the precise step of the Pol II transcription cycle that is modulated by the dosage compensation mechanism, we generated averaged metaprofiles of Pol II occupancies for the male autosomal and X-chromosomal genes (Fig. 2A). For all chromosomes, there are prominent peaks of Pol II association at promoters, with maxima about 50 bp downstream of the TSS that reflect widespread promoter-proximal stalling of Pol II (*11*, *12*). We observed a factor of 2.2 enrichment in Pol II occupancies at the promoters of male X-linked genes relative to autosomal ones [Fig. 2, A (lower panel) and E, and fig. S5C]. Pol II levels were also higher by a factor of 2.3 throughout the transcribed regions of male X-linked genes [Fig. 2, A (lower panel) and E]. Similar results were obtained using the male-derived embryonic S2 cell line (table S1 and fig. S5, A and D).

To account for the potential influences of gene-specific regulation, we compared these profiles against female controls by generating Rpb3 ChIP-seq profiles in female third-instar larva salivary glands. In contrast to males, the female pattern of Pol II occupancies was similar for both X-linked and autosomal genes (Fig. 2, B and E, and fig. S5C). The X-to-autosomal enrichment of Pol II occupancy at promoters was on average higher in males than in females by a factor of 1.9 (Fig. 2E). In gene-by-gene comparisons of promoter occupancies, male X-linked genes showed a significant shift toward higher rankings relative to females (Fig. 2C, $P < 2.2 \times 10^{-16}$). This increase in Pol II levels was maintained beyond the promoters, through the transcribed regions (factor of 2.2 increase) and 3′ ends (factor of 2.3 increase) of male X-linked genes. The results are robust: Analysis using a larger set of

[1]Max Planck Institute of Immunobiology and Epigenetics, 79108 Freiburg im Breisgau, Germany. [2]EMBL European Bioinformatics Institute, Wellcome Trust Genome Campus, Cambridge CB10 1SD, UK. [3]Okinawa Institute of Science & Technology, 1919-1 Tancha, Onna-son, Kunigami-gun, Okinawa 904-0495, Japan. [4]London Research Institute, Cancer Research UK, 44 Lincoln's Inn Fields, London WC2A 3LY, UK. [5]UCL Genetics Institute, Department of Genetics, Evolution and Environment, University College London, London WC1E 6BT, UK.

*These authors contributed equally to this work.
†To whom correspondence should be addressed. E-mail: luscombe@ebi.ac.uk (N.M.L.); akhtar@immunbio.mpg.de (A.A.)

Fig. 1. Pol II enrichment on the hyperacetylated male X chromosome. (**A**) Heat map of MOF binding and H4K16ac across genes in male (left) and female (right) samples. Genes are divided into three groups according to male wild-type H4K16ac levels: fully acetylated X-linked genes (top, 242 genes), promoter-acetylated autosomal genes (middle, 1157 genes), and nonacetylated autosomal genes (bottom, 203 genes). The TSS is indicated by a dashed line. Only expressed genes with significant Pol II signal in their transcribed region are shown. (**B**) Heat map showing male versus female differences (log2) in Pol II occupancies in the promoter (TSS −300 bp to TSS +500 bp) (left), transcribed regions (TSS +500 bp to PolyA −500 bp, scaled to the same length) (center), and 3′ ends (PolyA −500 bp to PolyA +300 bp) (right).
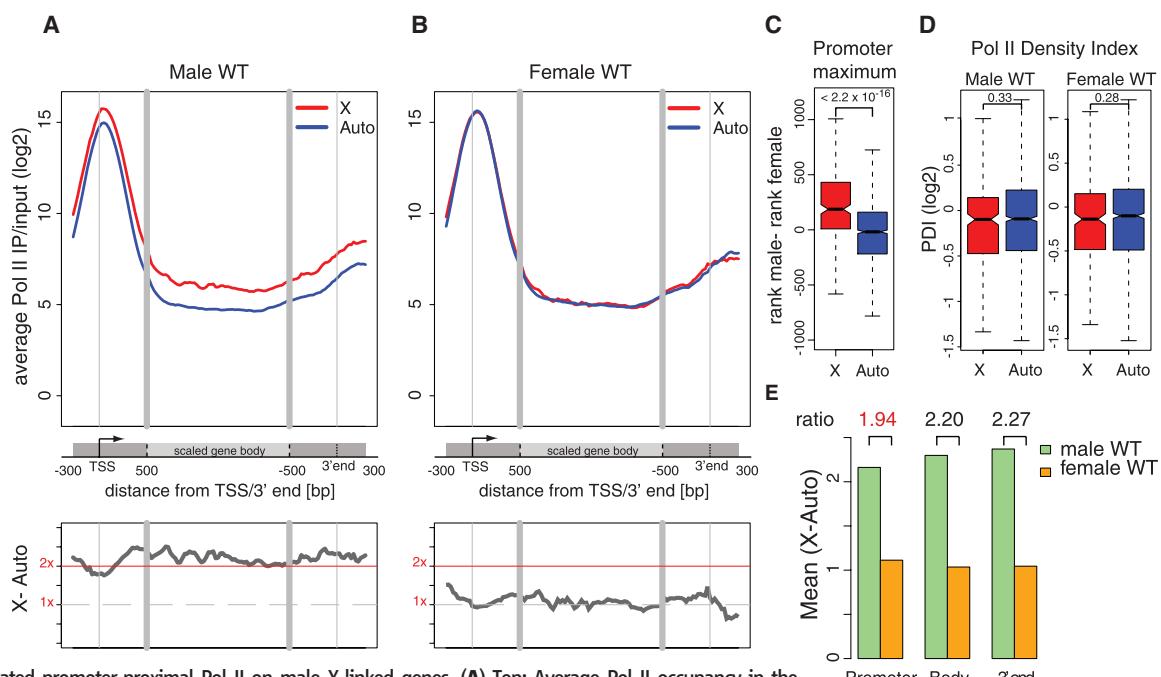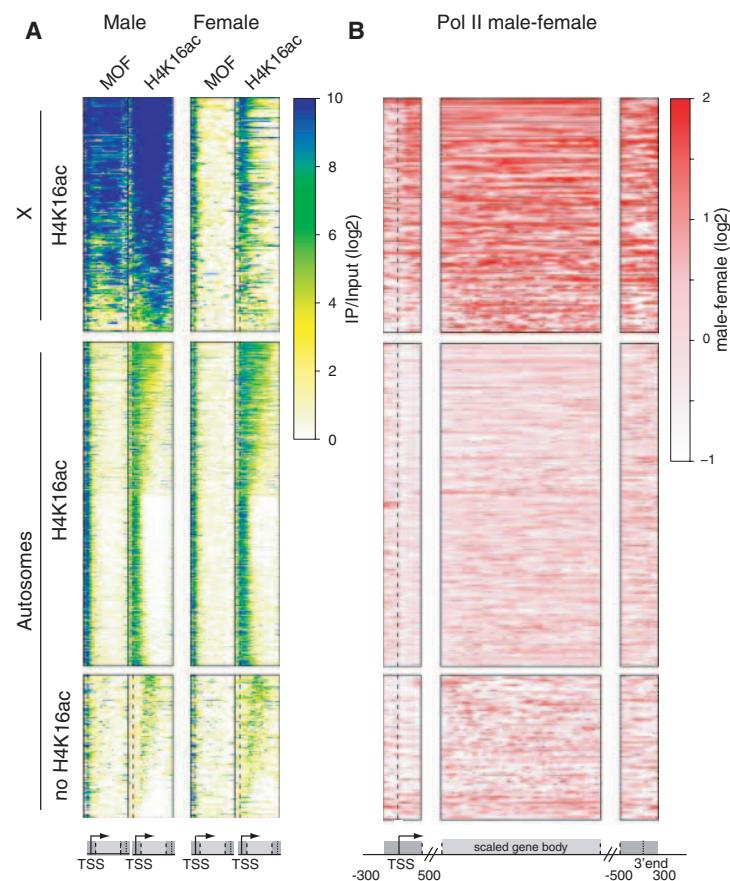
Fig. 2. Elevated promoter-proximal Pol II on male X-linked genes. (**A**) Top: Average Pol II occupancy in the promoter, middle, and 3′ end of X-linked (red) and autosomal (blue) genes in wild-type (WT) males. Bottom: Relative difference between the two profiles. Thin gray lines represent the TSS and PolyA sites, respectively. Expressed genes with significant Pol II signals in their transcribed regions are included (254 X-linked and 1414 autosomal genes for the promoter and gene body; 96 X-linked and 406 autosomal genes for the 3′ end, because 3′ ends with neighboring genes were excluded). (**B**) Same analysis for wild-type females. (**C**) Gene-by-gene comparison of Pol II occupancies. Box plots show male versus female differences in rank orders of maximal Pol II occupancies at promoters. (**D**) Box plots of Pol II density indices (PDIs) for genes in male and female samples. (**E**) Bar plots comparing the mean X versus autosome Pol II occupancy ratios in wild-type males and females at the promoter, middle, and 3′ end of genes. Indicated at top are the male versus female ratios of X-to-autosome Pol II occupancies. P values (Wilcoxon rank-sum test) are indicated in the box plots.

genes defined as expressed by microarrays and displaying significant Pol II signals at their promoters (639 X-linked and 3178 autosomal)—irrespective of significant ChIP-seq signal in gene bodies—revealed a factor of 2.0 increase in promoter-proximal Pol II occupancies among male X-linked genes (Fig. 3A). Analogous results were also obtained when genes were stratified by their expression levels (fig. S6 and table S2). Further, X-chromosomal promoters that were also acetylated in females (214 genes) showed a factor of 2.1 increase in Pol II occupancies in males (fig. S7, A, B, and D); the enhanced Pol II recruitment to these promoters correlated with a male-specific increase in H4K16ac upstream of the TSS (fig. S7, E and F). Absolute measurements of Pol II occupancy by quantitative polymerase chain reaction (qPCR) at individual gene

promoters validated the genome-wide observations (Fig. 3C).

Any regulatory effects at the level of Pol II recruitment should also influence initiated but transcriptionally stalled polymerases (11–13). In agreement with this, we observed a factor of 2.0 enrichment in Pol II occupancies at the promoters of stalled X-linked genes in males (Fig. 3C). This suggests that the dosage compensation mechanism operates in the absence of productive elongation.

More than one-third of *Drosophila* genes give rise to short (35- to 60-nucleotide) 5′ RNA transcripts that reside within—and indicate the presence of—fully initiated but temporarily stalled Pol II (13). Using a panel of 15 stalled genes, we measured an average factor of 2.1 increase in the production of short transcripts from male X-linked

promoters relative to females (Fig. 3D). To test the specificity of these assays, we checked that the qPCR reactions generated unique products of expected sizes and confirmed the absence of confounding mRNA fragments (Fig. 3D and table S3). A further 15 actively transcribed genes displayed an average factor of 1.7 increase in short RNA production from male X-linked promoters (fig. S8). These results provide strong evidence for enhanced transcription initiation in the hyperacetylated environment of the male X chromosome.

A previous study generated global run-on sequencing (GRO-seq) data in male S2 cells to report elevated transcription elongation among X-linked genes (8). To assess whether there are any changes in Pol II occupancies along the transcribed length of genes, we calculated a Pol II
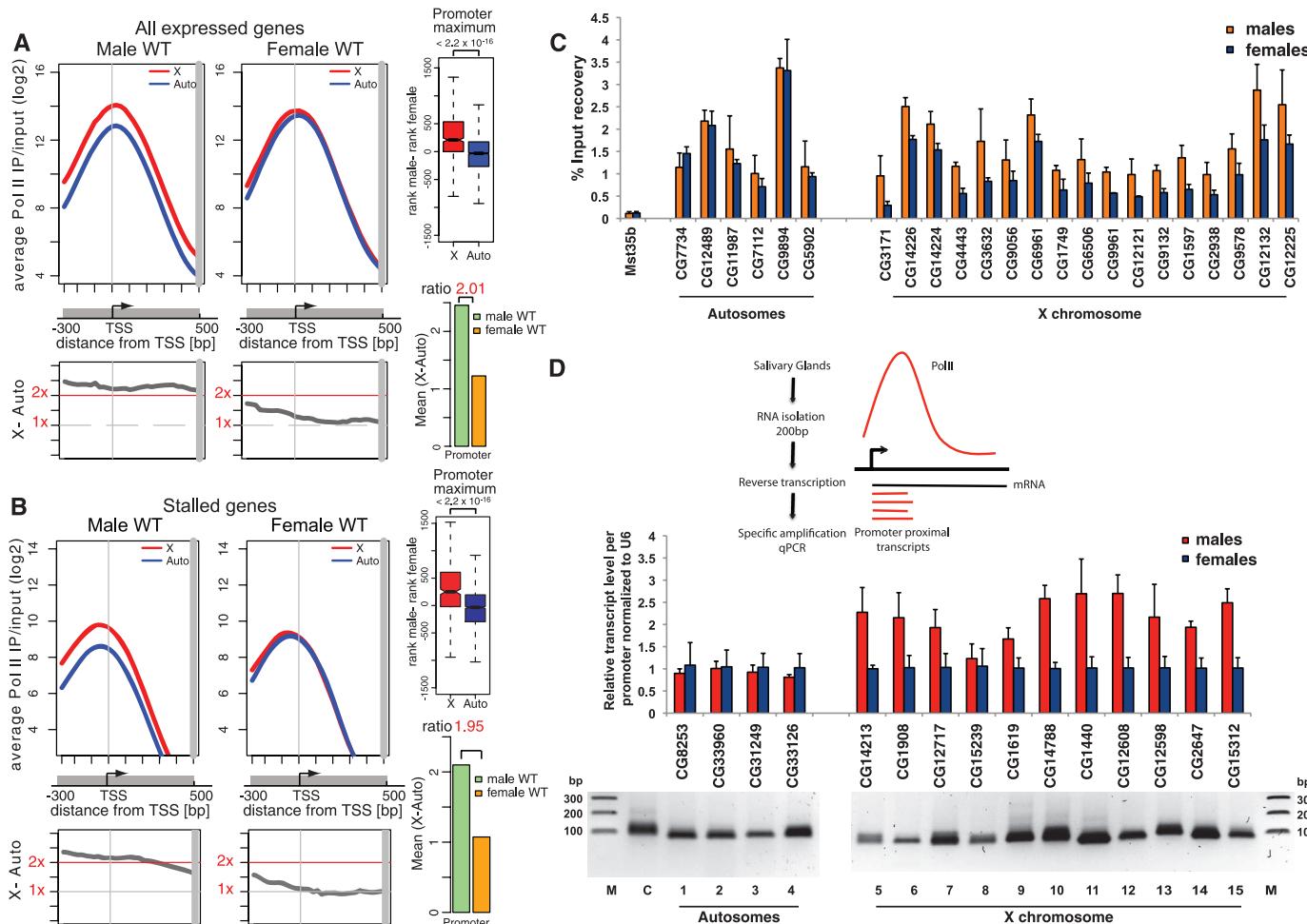
Fig. 3. Enhanced promoter activity is a general feature of X-linked genes. (**A**) Average Pol II occupancy around the TSS (TSS −300 bp, TSS +500 bp) using all expressed X-linked genes (red, 639 genes) and autosomal genes (blue, 3178 genes) in males and females. Box plots show male versus female differences in rank orders of maximal Pol II occupancies at promoters. Bar plots compare the mean X versus autosome Pol II occupancy ratios in males and females. (**B**) Same analysis for stalled genes, defined as unexpressed genes with significant Pol II occupancy at the promoter (395 X-linked and 1914 autosomal genes). (**C**) ChIP-qPCR validations in males and females. Pol II levels were measured as percent input recovery at 6 autosomal (left) and 17 X-linked gene promoters (right). The testis-specific *Mst35b*

gene serves as a negative control. Male X-linked promoter occupancy is elevated on average by a factor of 1.8. Error bars represent SD of three independent replicates. (**D**) Top: Short promoter-proximal RNAs were isolated, reverse-transcribed, and specifically quantified by qPCR. Middle: Relative transcript levels were measured for 15 transcriptionally stalled X-linked and autosomal genes. Error bars represent SD of three independent replicates. Bottom: Quality control for the specificity of short RNA detection using DNA gels with single product amplification. M indicates the molecular weight size marker; C indicates control U6 RNA. Note that a 64-bp DNA linker is added during reverse transcription to allow detection with a universal reverse primer. *P* values (Wilcoxon rank-sum test) are indicated in the box plots.

density index (PDI) as the ratio between total Pol II occupancies in the last three quarters versus the first quarter of the gene body (see supplementary materials). In contrast to expectations, our ChIP-seq data revealed similar PDI values for all chromosomes in both salivary glands and S2 cells (Fig. 1B, Fig. 2D, and fig. S5B). Moreover, in agreement with a recent report (*14*), reanalysis of the GRO-seq data above shows that transcriptional activities along gene bodies are equivalent for all large chromosomal arms (Fig. 4A), except for chromosome 3R and the heterochromatic chromosome 4. The differences in PDIs between the X chromosome and autosomes that remain after excluding the unusual chromosome 4 are resistant to MSL2 depletion (Fig. 4B). However, in support of our observations, reanalysis of the GRO-seq results using the same gene set as the ChIP-seq analysis in S2 cells (846 X-linked and 3869 autosomal) confirms the significantly

enhanced activity of X-linked promoters (figs. S5E and S9A).

To test whether enhanced Pol II recruitment to X-linked promoters is MSL-dependent, we performed Rpb3 ChIP-seq after RNA interference (RNAi)–mediated down-regulation of MSL2 in male salivary glands (figs. S1C and S3C). Promoter-proximal Pol II occupancies on the X chromosome were reduced by a factor of 1.8 to near-autosomal levels (Fig. 4, C, D, and F, and fig. S5C), and Pol II levels in gene bodies were decreased by a factor of 1.9 (Fig. 4F). Analogous results were obtained for different gene sets (fig. S10). That the loss of compensation was incomplete probably reflects gene-specific transcriptional buffering and gene-specific feedback regulation in the absence of MSL-mediated dosage compensation (*15*). In agreement with previous observations, this buffering was more evident for weakly expressed genes (table S2) (*15*). MSL2 depletion

also caused a general decrease in Pol II densities along the transcribed region of genes (Fig. 4E); however, all chromosomes were similarly affected, suggesting a secondary effect unrelated to dosage compensation.

Taken together, our data suggest that dosage compensation mainly arises from a near-doubling of Pol II activity at the promoters of male X-linked genes, most likely reflecting enhanced transcription initiation on the male X chromosome. In addition, release of Pol II into gene bodies is also slightly enhanced, which suggests that the transition into elongation might be facilitated. An initiation-based model readily explains the recent observation that the promoter sequence and associated transcription factor–binding sites influence the susceptibility of a reporter to dosage compensation (*16*). It is also consistent with the global hyperacetylation of male X-linked promoters and intergenic regions, which elevates the general accessibility of regulatory
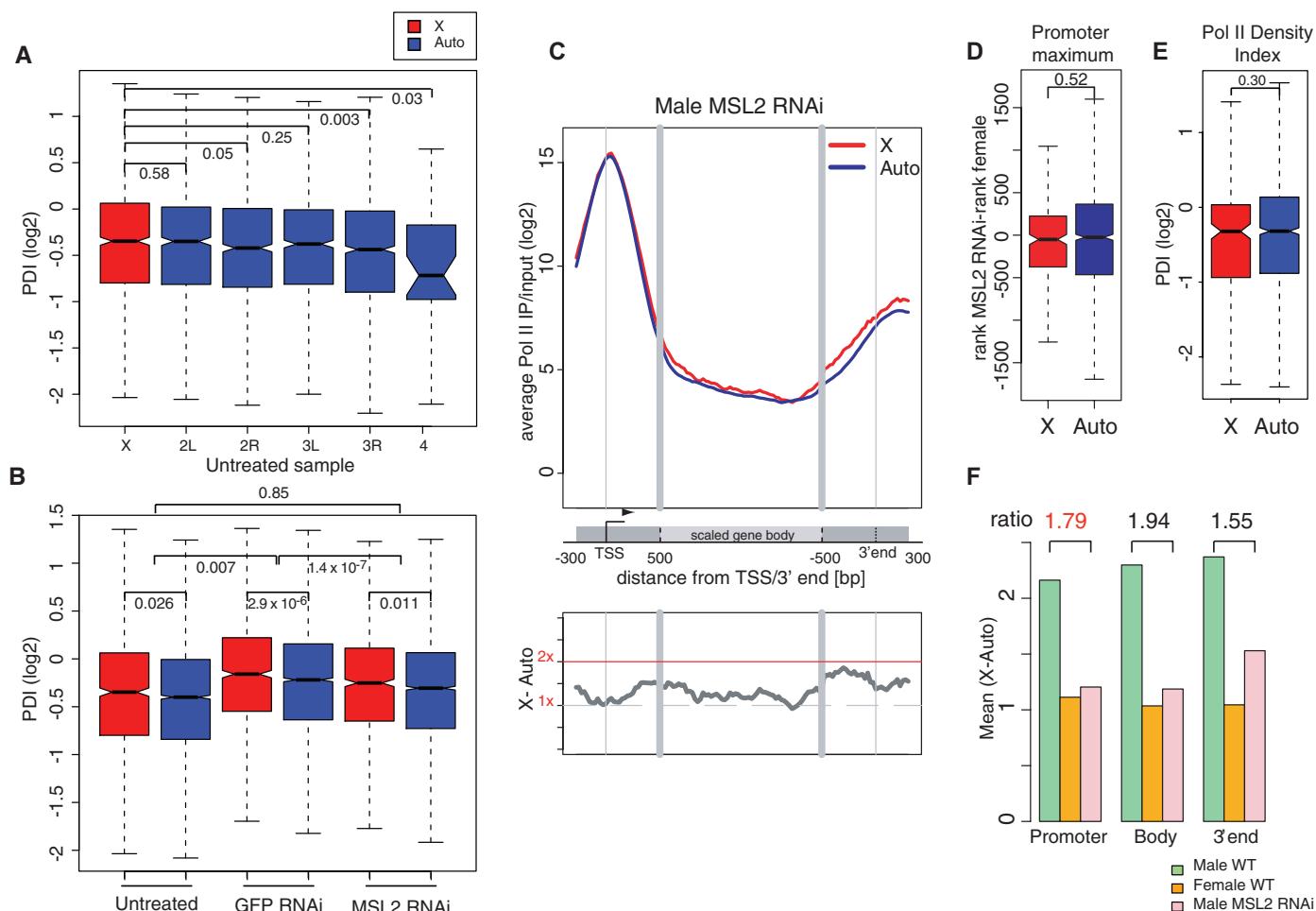
Fig. 4. Enhanced promoter activity is dependent on the MSL complex. (**A**) Box plots show the distribution of PDI values (log$_2$) for each chromosome arm using publicly available GRO-seq data derived from S2 cells by Larschan *et al.* (*8*). (**B**) Box plots show the distribution of PDI values (log$_2$) for X-linked genes (red) and autosomal genes (blue) in untreated, green fluorescent protein (GFP)–treated, and MSL2 RNAi–treated S2 cells using GRO-seq data by Larschan *et al.* (*8*). Genes on the heterochromatic chromosome 4 have been removed. (**C**) Top: Average Pol II occupancy in the promoter, middle, and 3′ end of X-linked (red) and autosomal (blue) genes in MSL2 RNAi males detected by ChIP-seq against Rpb3 (this study). Bottom: Relative difference between the two profiles. The same genes as in Fig. 2A were used. (**D**) Box plots show MSL2 RNAi male versus female differences in rank orders of maximal Pol II occupancies at promoters. (**E**) Box plots of PDI values for genes in MSL2 RNAi male and female samples. (**F**) Bar plots comparing the mean X versus autosome Pol II occupancy ratios in wild-type males and females and MSL2 RNAi males at the promoter, middle, and 3′ end of genes. Indicated at top are the wild-type male versus MSL2 RNAi ratios of X-to-autosome Pol II occupancies. *P* values (Wilcoxon rank-sum test) are indicated in the box plots.

sequences to the transcriptional machinery (*2*, *5*). At the same time, hyperacetylation within gene bodies is a prerequisite for MSL complex binding to the transcribed regions of X-linked genes (*1*). Restricting the MSL complex to these sites may prevent the physical obstruction of promoters in males and thereby help to balance the transcriptional output between sexes.

References and Notes

1. T. Conrad, A. Akhtar, *Nat. Rev. Genet.* **13**, 123 (2012).
2. M. E. Gelbart, E. Larschan, S. Peng, P. J. Park, M. I. Kuroda, *Nat. Struct. Mol. Biol.* **16**, 825 (2009).
3. F. N. Hamada, P. J. Park, P. R. Gordadze, M. I. Kuroda, *Genes Dev.* **19**, 2289 (2005).
4. T. Straub, G. D. Gilfillan, V. K. Maier, P. B. Becker, *Genes Dev.* **19**, 2284 (2005).
5. O. Bell *et al.*, *Nat. Struct. Mol. Biol.* **17**, 894 (2010).
6. S. W. Park, H. Oh, Y. R. Lin, Y. Park, *Biochem. Biophys. Res. Commun.* **399**, 227 (2010).
7. J. C. Lucchesi, *Curr. Opin. Genet. Dev.* **8**, 179 (1998).
8. E. Larschan *et al.*, *Nature* **471**, 115 (2011).
9. T. Conrad *et al.*, *Dev. Cell* **22**, 610 (2012).
10. J. Kind *et al.*, *Cell* **133**, 813 (2008).
11. J. Zeitlinger *et al.*, *Nat. Genet.* **39**, 1512 (2007).
12. G. W. Muse *et al.*, *Nat. Genet.* **39**, 1507 (2007).
13. S. Nechaev *et al.*, *Science* **327**, 335 (2010).
14. A. M. Johansson, P. Stenberg, A. Allgardsson, J. Larsson, *Mol. Cell. Biol.* **32**, 2121 (2012).
15. J. H. Malone *et al.*, *Genome Biol.* **13**, r28 (2012).
16. C. Laverty, F. Li, E. J. Belikoff, M. J. Scott, *PLoS ONE* **6**, e20455 (2011).

Fate-Restricted Neural Progenitors in the Mammalian Cerebral Cortex

Santos J. Franco, Cristina Gil-Sanz,* Isabel Martinez-Garay,*† Ana Espinosa, Sarah R. Harkins-Perry, Cynthia Ramos, Ulrich Müller‡

During development of the mammalian cerebral cortex, radial glial cells (RGCs) generate layer-specific subtypes of excitatory neurons in a defined temporal sequence, in which lower-layer neurons are formed before upper-layer neurons. It has been proposed that neuronal subtype fate is determined by birthdate through progressive restriction of the neurogenic potential of a common RGC progenitor. Here, we demonstrate that the murine cerebral cortex contains RGC sublineages with distinct fate potentials. Using in vivo genetic fate mapping and in vitro clonal analysis, we identified an RGC lineage that is intrinsically specified to generate only upper-layer neurons, independently of niche and birthdate. Because upper cortical layers were expanded during primate evolution, amplification of this RGC pool may have facilitated human brain evolution.

The mammalian cerebral cortex consists of six major layers that each contain specific subtypes of neurons characterized by distinct projection patterns and gene expression profiles (*1*). These layer-specific classes of cortical excitatory neurons are derived from radial glial cells (RGCs) in sequential order, with neurons destined for lower layers being generated first, followed by upper-layer neurons and, finally, cortical astrocytes (*1*). This relationship between birthdate and laminar fate of neurons in the cerebral cortex has been documented for more than 50 years, although it has remained unclear whether cell fate is determined directly by birthdate (*2*) or if the two are linked more indirectly rather than causally (*3*).

RGCs divide asymmetrically in the cortical ventricular zone to self-renew and generate neurons directly or, more commonly, indirectly via intermediate progenitor cells that divide symmetrically in the ventricular and subventricular zones (*4*). The transcription factor Cux2 is expressed specifically in neurons in upper layers II to IV in the mature cortex (Fig. 1A), but also in intermediate progenitors in the developing subventricular zone (*5*, *6*), suggesting that upper-versus lower-layer fate might be determined before neuronal differentiation. We found that Cux2 mRNA is also expressed in the ventricular zone in a salt-and-pepper manner (Fig. 1B and fig. S1, A to D), indicating that some RGCs may be committed to generate upper-layer neurons. To establish the identity of ventricular zone Cux2$^+$ cells and to determine their lineage potential, we employed genetic fate mapping using a mouse strain expressing Cre recombinase from the *Cux2* locus (*7*). Crossing the *Cux2-Cre* driver line to reporter mouse lines led to recombination primarily in upper-layer neurons in the mature cortex, with 76% of recombined cells occupying layers II to IV (Fig. 1C and fig. S1, E to H). Only 17 and 7% of recombined cells were found in lower layers V and VI, respectively (Fig. 1C and fig. S1, E to H), and most of these were Satb2$^+$ excitatory neurons (74%) (fig. S1, I and J), which form callosal projections similar to layer II and III neurons (*8*, *9*). The remainder were Gad65/67$^+$ interneurons (26%) (fig. S1, I and J) derived from the ganglionic eminences, in agreement with previous observations (*6*). Furthermore, in the developing cortex we identified clonal columns of recombined cells in the ventricular zone (Fig. 1D), resembling the pattern of endogenous Cux2 mRNA expression. The majority of recombined cells in the ventricular zone expressed the RGC markers Pax6 (Fig. 1E) and nestin (Fig. 1F), but not the intermediate progenitor marker Tbr2 (Fig. 1G). Recombined cells divided at the ventricular surface (Fig. 1, H and I), maintained apical and basal processes, and underwent interkinetic nuclear migration (Fig. 1I), all hallmarks of ventricular zone RGCs. These results suggest that a subset of RGCs are restricted in their lineage potential.

To further analyze the relationship between Cux2$^+$ RGCs and their offspring, we introduced a Cre reporter plasmid into RGCs in *Cux2-Cre* embryos by in utero electroporation. In this FLEx (FLip-Excision) technology–based reporter plasmid (*10*), Cre recombination switches expression from tdTomato fluorescent protein to green fluorescent protein (GFP), thereby permitting differential fluorescent labeling of Cux2$^+$ and Cux2$^-$ RGCs and their offspring (Fig. 2A). Electroporation of the reporter at embryonic day (E) 12.5 and analysis at E13.5 demonstrated that a subset of electroporated RGCs had recombined the reporter and turned on GFP (Fig. 2B), even though at this early time point the tdTomato signal remained because of protein perdurance. At postnatal day (P) 10, 83% of neurons with recombined reporters (GFP$^+$) had settled in upper layers II to IV (Fig. 2, C and D), whereas only 7% of the neurons with nonrecombined reporters (tdTom$^+$GFP$^-$) were located in upper layers (Fig. 2, C and D). These results suggest that the Cux2$^+$ progenitors constitute a lineage largely fated to become upper-layer neurons with a small contribution to lower layers, whereas the Cux2$^-$ lineage primarily generates lower-layer neurons.

To facilitate temporal fate mapping of the Cux2$^+$ lineage, we generated a mouse line in which the tamoxifen-inducible *CreERT2* (*11*) gene is knocked into the endogenous *Cux2* locus (fig. S2, A to C). By crossing *Cux2-CreERT2* mice with a Cre-reporter strain and inducing recombination

Dorris Neuroscience Center and Department of Cell Biology, The Scripps Research Institute, 10550 North Torrey Pines Road, La Jolla, CA 92037, USA.

*These authors contributed equally to this work and are listed alphabetically.
†Present address: Department of Physiology, Anatomy, and Genetics, University of Oxford, Oxford OX1 3QX, UK.
‡To whom correspondence should be addressed. E-mail: umueller@scripps.edu